

Growth and characterization of ultrathin Fe magnetic layers deposited on atomically clean Si(001) by molecular beam epitaxy

N.G. Gheorghe*, M.A. Husanu, G.A. Lungu, D. Macovei, V. Kuncser, R.M. Costescu, D.G. Popescu, C.M. Teodorescu

National Institute of Material Physics Bucharest-Magurele, Atomistilor 105b, 077125 Magurele-Ilfov Romania

*corresponding author: e-mail nicoleta.gheorghe@infim.ro

Abstract

We present the very first surface physics experiments performed in ultrahigh vacuum (UHV) in Romania. A technology for cleaning Si(001) wafers was achieved by using annealing at 900-1000°C in UHV. Fe layers grown on the Si(001) single crystal surface are characterized by low energy electron diffraction, reflection high energy electron diffraction, and Auger electron spectroscopy. The clean sample contamination and the interface reactivity are assessed by these combined techniques, whereas magnetism of Fe is investigated by magneto-optical Kerr effect. Higher deposition temperatures yield better surface ordering, but also enhance Fe and Si interdiffusion and decrease the Fe magnetic moment.

1. Introduction

A key test of most surface science UHV apparatuses, and especially of MBE installations, is the cleaning of semiconducting samples, of which Si(111) and Si(001) are the most used examples. This allows the setup and commissioning of standard characterization devices, such as (i) for structural characterization: LEED, RHEED; (ii) for chemical characterization: AES, XPS. Usually, silicon substrates are prepared by flashes at very high temperatures (1200 – 1400°C) [1-3], cycles of Ar⁺ sputtering and annealing [4-6], cleavage under UHV [7], RCA (Radio Corporation of America) method and other wet chemical methods [8-9], gas source MBE [10], laser ablation [11-12]. Any of these methods has specific disadvantages. Sputtering introduces defects, very high temperature flashes induces the risk of melting the sample, cleavage is rarely reproducible, gas source MBE is using high risk gases, etc.

In this paper we investigate a novel and cheap method for preparing atomically clean samples of Si(001) just by annealing in ultrahigh vacuum. Once established, the method may be repeated several times with reproducible results in obtaining low-contamination, well characterized surfaces of Si(001). The characterization was mainly performed by LEED and AES, but also RHEED was used for investigating the cleanliness of the sample and the surface reconstruction. Consistent investigation and analysis of AES allowed derivation of the kinetics of contamination and the nature of the reacted compounds formed at the surface.

Iron layers deposited on silicon have been subject of numerous investigations in the past, since this interface involves both the most common pure ferromagnetic metal and the most used semiconductor in the industry. One of the global aims of our research is to provide recipes for fabrication of ferromagnetic contacts on semiconductors for spin injection. However, spin injection efficiency is strongly dependent on the reactivity at interface. At the same time, the magnetism of the layers is strongly perturbed by the interface reactivity [13].

In the present paper we will address Fe/Si(001) interfaces, for which fewer studies combining reactivity with magnetism are reported up to the present moment.

When the Fe deposition is performed at room temperature, Si diffusion into the Fe film promotes a layer of approximate composition Fe_3Si [14], which becomes ferromagnetic for coverages exceeding $3.6 \text{ ML} \approx 5 \text{ \AA}$ [15] or about 7 \AA [16-17].

The aim of this paper is to investigate the long- and short-range ordering, composition and magnetic properties of Fe deposited onto Si(001) in order to see which are the correlations between magnetic properties, interface reactivity and local atomic order. The long-range order was investigated by LEED, the chemical reactivity and the intermixing by Auger electron spectroscopy (AES), and the magnetic properties by magneto-optical Kerr effect (MOKE).

2. Experimental aspects

2.1. Description of the experimental cluster for Surface and Interface Science

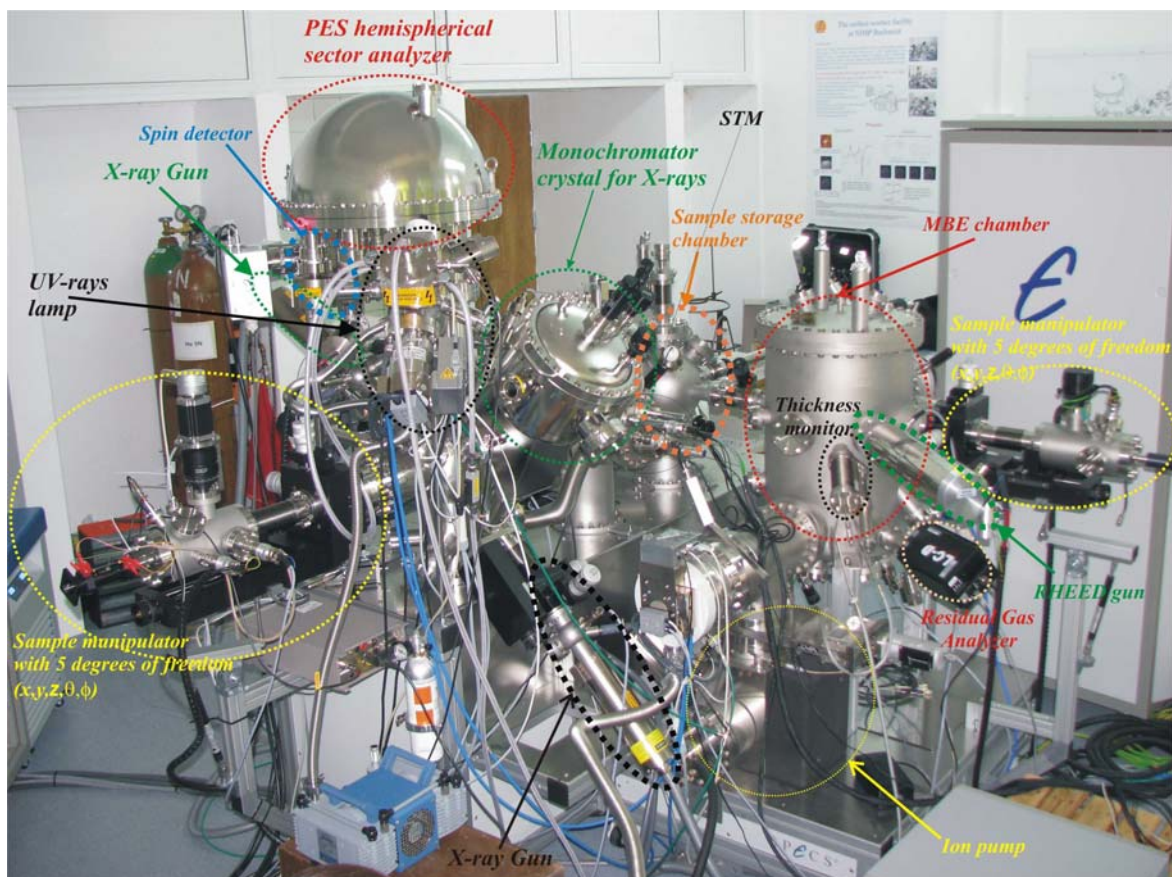
The Cluster represents one of the most complex such systems in Europe, makes possible the preparation and characterization *in situ* of surfaces and interfaces, and consists of four units, of which the first three are mutually coupled (Fig. 1):

- The MBE (Molecular Beam Epitaxy) Chamber
- The STM (Scanning Tunneling Microscope) Chamber

- The Spin- and Angle-resolved Photoelectron Spectroscopy (SARPES)
- The PEEM (Photoemission Electron Microscopy) and LEEM (Low Energy Electron Microscopy) System.

All devices operate in ultra-high vacuum ($1-2 \times 10^{-10}$ mbar). It is possible to perform *in situ* characterization by low energy electron diffraction (LEED), reflection high energy electron diffraction (RHEED), Auger electron spectroscopy (AES), quadrupole mass spectroscopy (QMS), classical and high-resolution X-ray photoelectron spectroscopy (XPS), ultraviolet photoelectron spectroscopy (UPS), etc.

The performance of the complex system described above is illustrated in Fig. 2 for high resolution photoelectron spectroscopy (line widths comparable to that obtained with synchrotron radiation sources) and in Fig. 3 for scanning tunneling microscopy with atomic resolution. Further, Fig. 4 shows the first results obtained for the visualization of the monatomic terraces of Si(001) by low energy electron microscopy (LEEM). The ultimate resolution achieved with the LEEM in darkfield mode is 4.1 nm (20-80 % criterion).



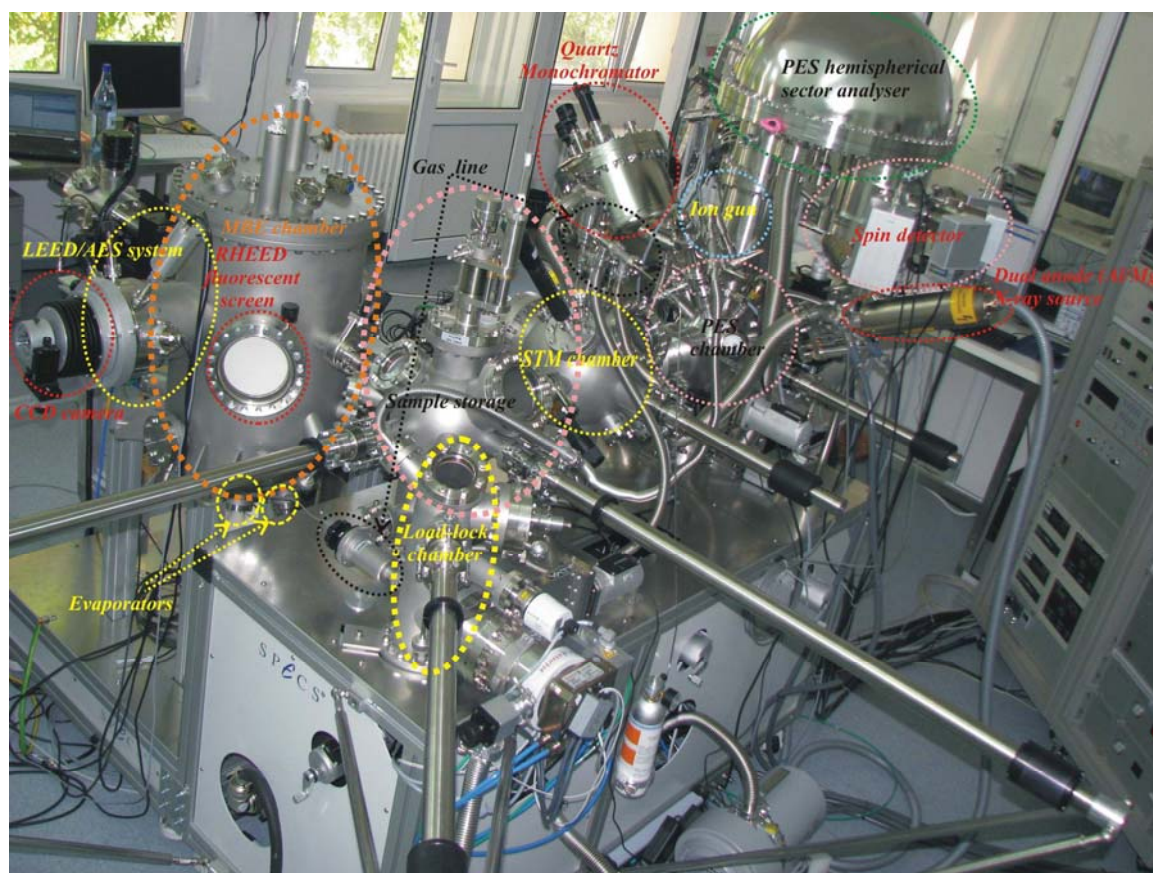


Fig. 1 Experimental measurement cluster for surface and interface science

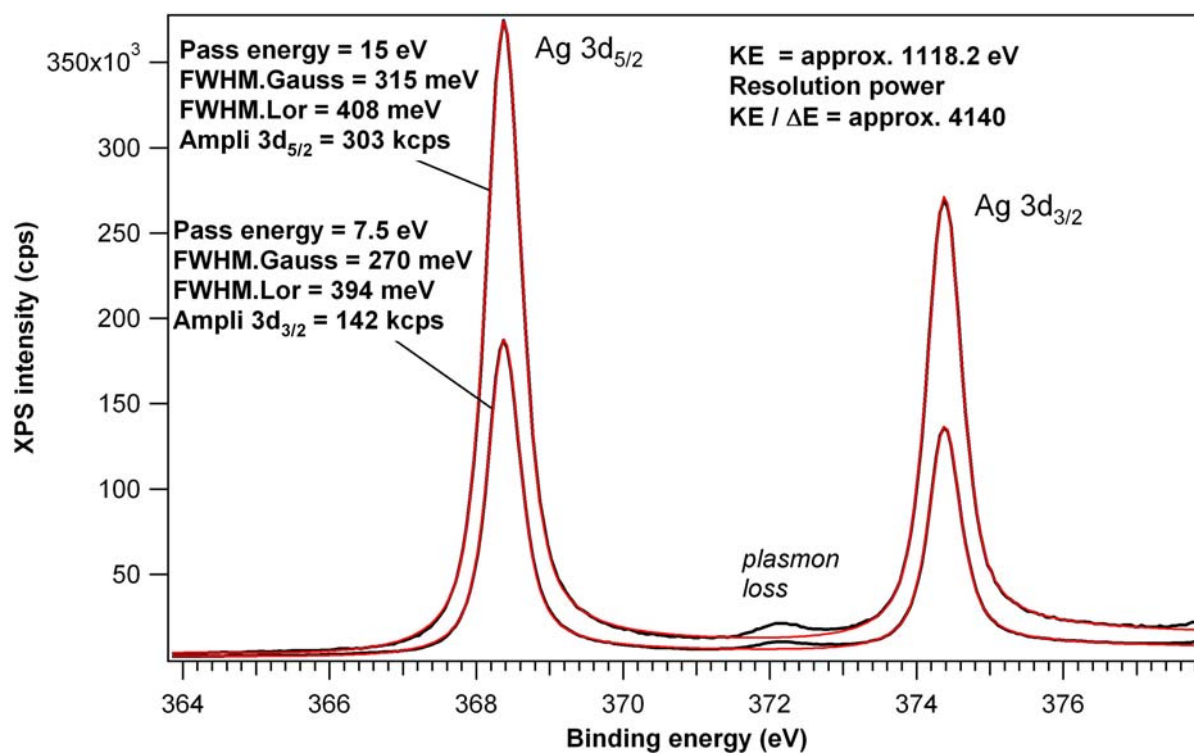


Fig. 2 High resolution XPS spectra for an Ag foil using a monochromatized X-ray source.

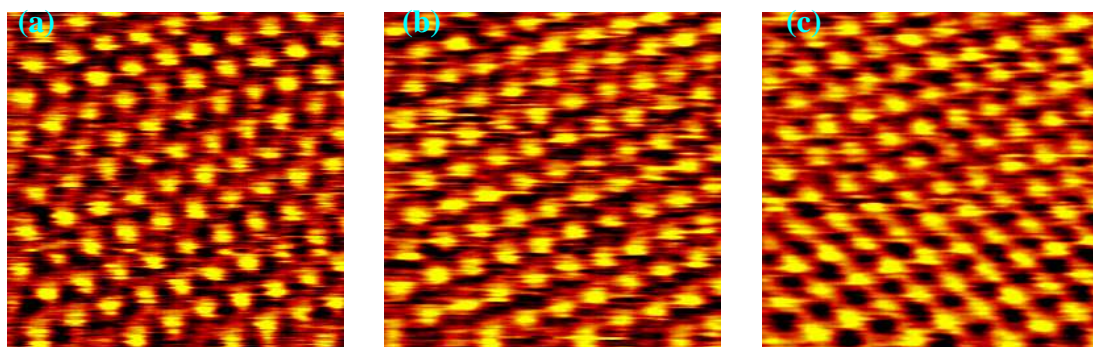


Fig. 3 Scanning Tunneling Microscopy (STM) images with atomic resolution obtained on highly oriented pyrolytic graphite (HOPG) (0001), with different tip voltages: (a) 630 mV; (b) 713 mV; (c) 884 mV.

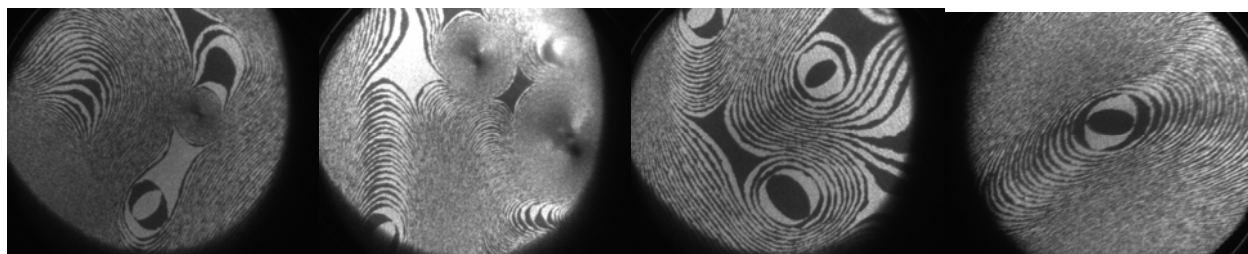


Fig. 4 LEEM darkfield images on one of the diffraction spots ($1/2, 0$) of the Si(001) surface reconstruction. The size of the image (field of view, FOV) is 3 μm .

In approximately 18 months of operation of the surface and interface facility, there has been a significant number of scientific papers published in ISI ranked journals with significant impact factor. To date, outstanding contributions using this setup were reported on catalytic systems [18-21], oxides with photocatalytic or diluted magnetic behavior [22-26], nanoparticle systems [27-28], ferroelectrics [29-30], silicon carbide/silica heterostructures [31], hydrogen storage materials [32].

2.2. Preparation of atomically clean Si(001)

Two-domain Si(001) single crystal wafers were cleaned by repeated cycles of annealing at 900-1000°C. The typical time of an annealing step is 30 mins. The composition of the residual gas was monitored with the QMS. After each cycle of annealing, the state of the surface contamination was checked by AES, and its crystallinity by LEED and RHEED. RHEED was proven to be a less surface sensitive technique: RHEED spots started to appear well before achieving the surface cleaning at atomic level. By contrast, LEED patterns were visible only

when the sample was almost clean. Also, only the clean sample showed visible RHEED lines, denoting a flat surface [13,33].

Achieving a LEED pattern also allowed inspection of the whole surface of the sample and practically the whole surface presents long range ordering. This was not the case with samples prepared by Ar^+ sputtering or by very high temperature annealing [1-2], where only a part of the sample presented a well-defined LEED pattern.

2.3. Growth of Fe layers by molecular beam epitaxy

Ultrathin Fe layers were prepared on atomically clean Si(001) in the molecular beam epitaxy chamber operating in the pressure range of low 10^{-10} mbar. The samples are investigated *in situ* by Auger electron spectroscopy (AES) (Fig. 5 presents AES survey spectra of the as-prepared Si(001) and of the 6.7 nm Fe deposition on Si(001), respectively) and low-energy electron diffraction (LEED). Single crystals of Si(001) were cleaned by heating Si(001) wafers at 1200 °C for 30 minutes in a vacuum not exceeding 5×10^{-9} mbar, then waiting for the vacuum recover back to low 10^{-10} mbar.

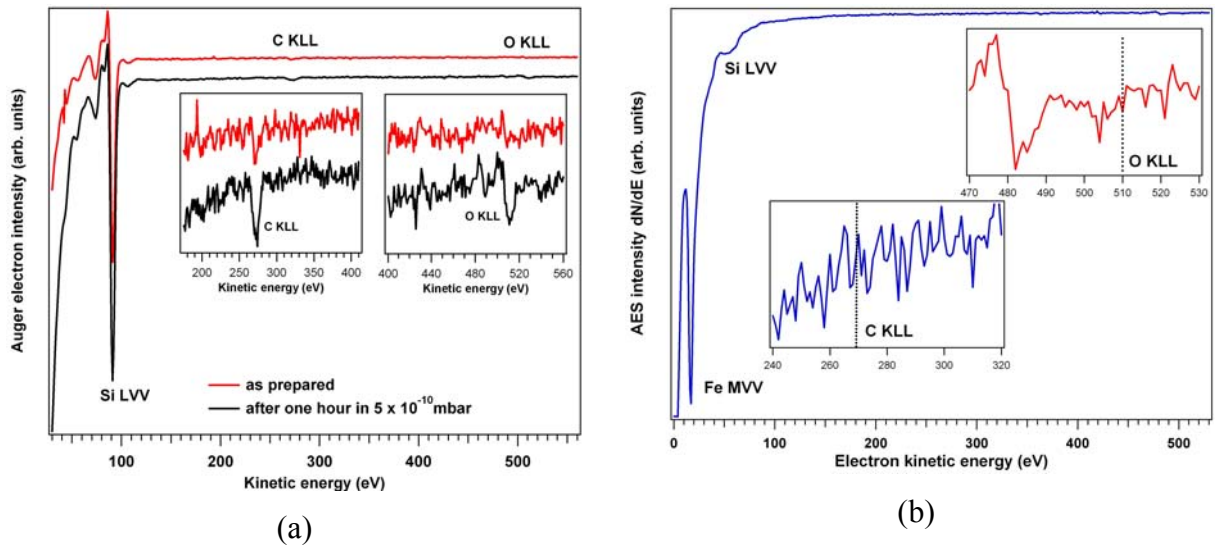


Fig. 5. Survey scans of Auger electron spectroscopy (a) on the as-prepared Si(001) sample and (b) on a layer of 6.7 nm Fe immediately after its deposition on Si(001).

Fe was evaporated from a Specs EBE-4 electron bombardment source at a rate of 0.06 Å/s and at normal incidence. The base pressure was in the low 10^{-9} mbar range during deposition. 1 monolayer (ML) of Fe is equivalent to about 1.43 Å, as indicated by the thickness monitor set with Fe parameters (density, Z-factor).

After the deposition, the samples were capped with 30 Å of Au (deposited also near normal incidence) and characterized *ex situ* by MOKE, using a setup manufactured by AMACC

Anderberg and Mod  r Accelerator AB. The maximum applied field was 0.6 T and the measurements were performed at room temperature.

3. Results and Discussions

3.1 Clean Si(001)

Fig. 6 presents AES recorded during the sample cleaning. We note a considerable shift of around 15 eV towards higher kinetic energies for the as-introduced sample. For instance, the Si-O peak results at 90 eV, value very close to the Si-Si peak of 92 eV, well known in literature [4,11], although some authors report slightly lower values: 91 eV [3,5] or even 90 eV [10]. We attribute this shift to the inherent contamination layer from the as-introduced sample, which behaves like an insulator and becomes charged by the primary electrons produced by the spectrometer. After the first annealing cycle, the Si⁰ line moves its position to 91-92 eV, whereas the oxidized Si⁴⁺ line shifts towards 78 eV, in good agreement with data from literature [3,5]. Subsequent annealing cycles do not change the situation drastically; whereas after the fourth annealing a diffuse LEED pattern appears and the Si LVV AES looks quite different (see Fig. 6). A last cycle of annealing resulted in the vanishing of the Si⁴⁺ (78 eV) line, a strong reinforcement of the Si⁰ (92 eV) line, and the disappearance of the oxygen KLL line (see Fig. 6, black curve). The carbon KLL line did not disappear, but decreased in intensity. By using Auger atomic sensitivity factors [34] it is estimated that the remaining carbon represents about 4 ± 2 % of a single atomic layer. It is possible that this contamination appears during the time interval between the achievement of the preparation procedure and the measuring of this line (15-20 mins. are elapsed between these two events).

At the end of the cleaning procedure, sharp LEED patterns were obtained, as evidenced in Fig. 2. Also, the spots belonging to both (2 × 1) and (1 × 2) reconstructions are quite well observed, since the wafer was not miscut so as to provide single domain reconstruction [35]. Fig. 8 presents the RHEED pattern obtained along the <110> axis on the clean sample. Although the mounting of the sample on the sample holder was such as no direct observation along the highest symmetry axis <100> was possible, the <110> RHEED also provided fractionary spots, which reconfirmed the (2 × 1) - (1 × 2) reconstruction of the surface.

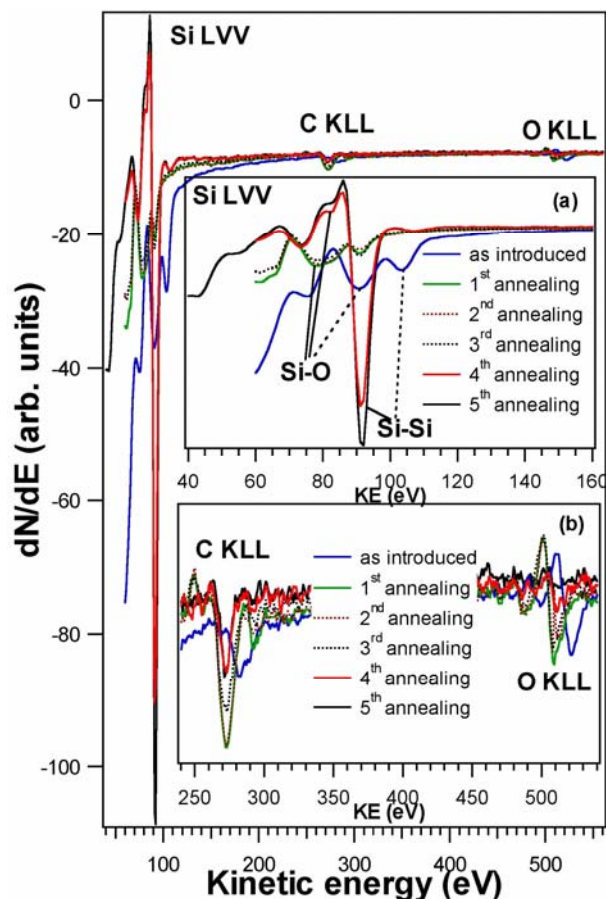


Fig. 6. Auger electron spectra of the Si(001) sample during the annealing cycles. Inserted are (a) detail of the Si LVV lines; (b) detail of the C KLL and O KLL lines.

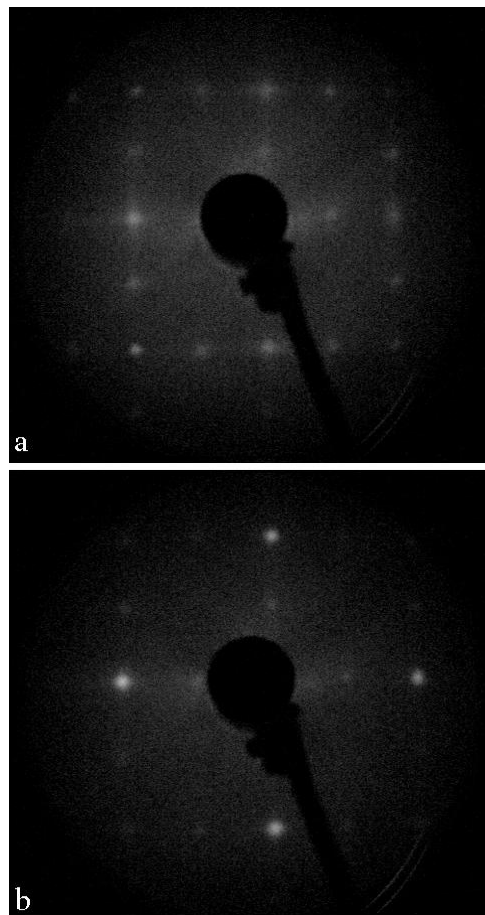
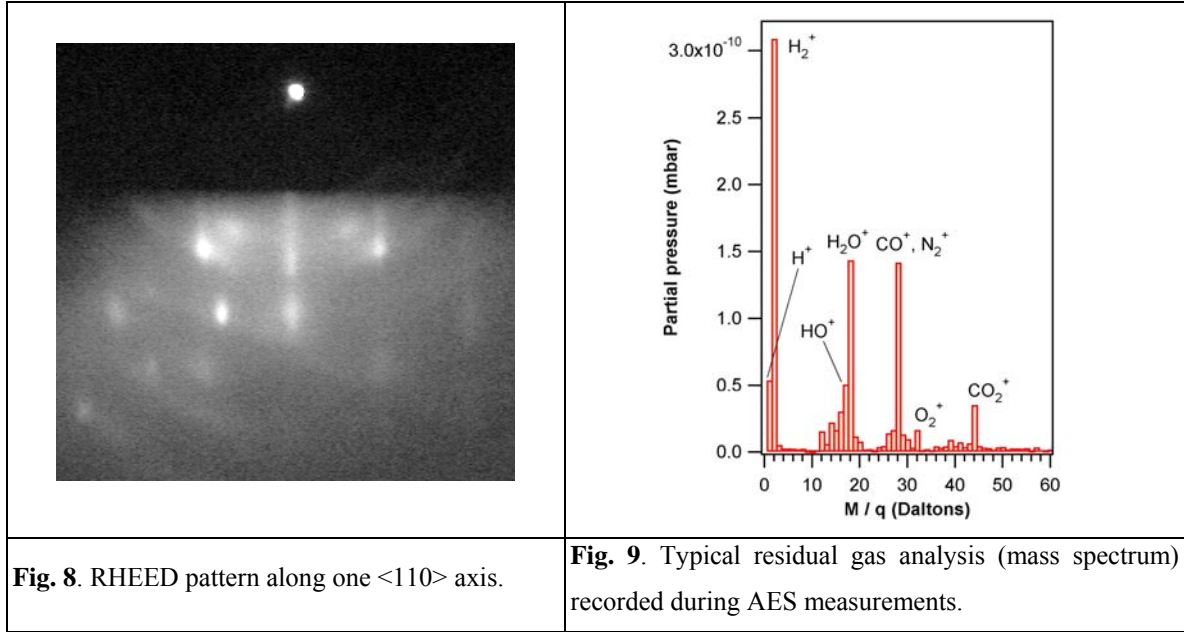


Fig. 7. LEED patterns obtained with primary electrons at 55.9 eV (a) and 43.8 eV (b). The (01) spots are the brightest ones from (b). One may also observe distinct (0 1/2) spots.

3.2. Surface contamination in ultrahigh vacuum

After successful preparation, the sample was measured continuously by AES. The composition of the residual gas during these measurements is represented in Fig. 9. The influence of these molecules results in contamination of the sample, as demonstrated in Fig. 10. The Si^0 LVV peak decreases in intensity, the Si^{4+} LVV peak (or oxidized silicon) starts to manifest [see Fig. 10(b)], whereas the carbon and oxygen KLL peaks increase [see Fig. 10(c)]. The contamination evolves by primary surface chemical reactions [7], but might also be induced by electron impact from the Auger spectrometer [3]. The next step was to plot the evolution of the intensity of the different peaks (Si^{4+} LVV, Si^0 LVV, C KLL and O KLL), versus time. Consequently, we had to introduce a curve fitting in order to derive the intensity, defined as the minimum value from which the maximum value is subtracted (resulting in a net negative value).



The peaks are asymmetric, therefore a deconvolution with a symmetric function, such as a Voigt profile [36] was not successful. In Fig. 10(c), the C and O Auger spectra were fitted by using an analytical approximation of the convolution of the Beutler-Fano profile with a gaussian lineshape accounting for the finite resolution of the spectrometer [37].

The use of the Beutler-Fano profile has the following explanation: the Auger effect is an autoionization process, result of a de-excitation of a discrete resonance (creation of a core hole) embedded in a continuum of multiparticle ionization [38]. In Fig. 11 the evolution of the five signals of interest (Si^{4+} LVV, Si^0 LVV, C KLL and O KLL) are represented as function of time. The data were fitted with exponential decays, such as $I(t) = I(0) + A \exp(-t / \tau)$. The resulting fitting parameters are represented in Table 1. We observe that the Si^{4+} LVV signal may be well approximated by a saturation formula of the type $\text{Const.} \times \{1 - \exp(-t / \tau)\}$ (note that Const. is a negative value), whereas the Si^0 LVV signal is better approximated by a formula on the type $\text{Const.} \times \{1 + \exp(-t / \tau)\}$. This is somehow confusing, since one expects that with infinite contamination (or time spent in the chamber) the clean surface signal should disappear completely. Also, from the carbon contamination one obtains that a C KLL signal of $-1.661 + 0.320 = -1.341$ units is inherently present on the sample from the very beginning. This produces a contamination of some $-1.341 / (-50.46 - 54.58) \approx 0.0128$, but this has to be multiplied with the ratio between the Auger sensitivity factors: 0.924 for Si LVV and 0.282 for C KLL [36]. This results in an overall contamination of $\sim 4.2\%$. Finally, the O KLL signal obeys a saturation-like law, but with a very long lifetime. This suggests that the well known Si^{4+} LVV signal at 78 eV may be due not only to formation of Si-O bonds (since therefore the lifetimes of this signal and

that of oxygen KLL should be similar), but rather to the formation of Si-CO complexes. Finally, we try to explain the unexpected behavior of the clean silicon signal.

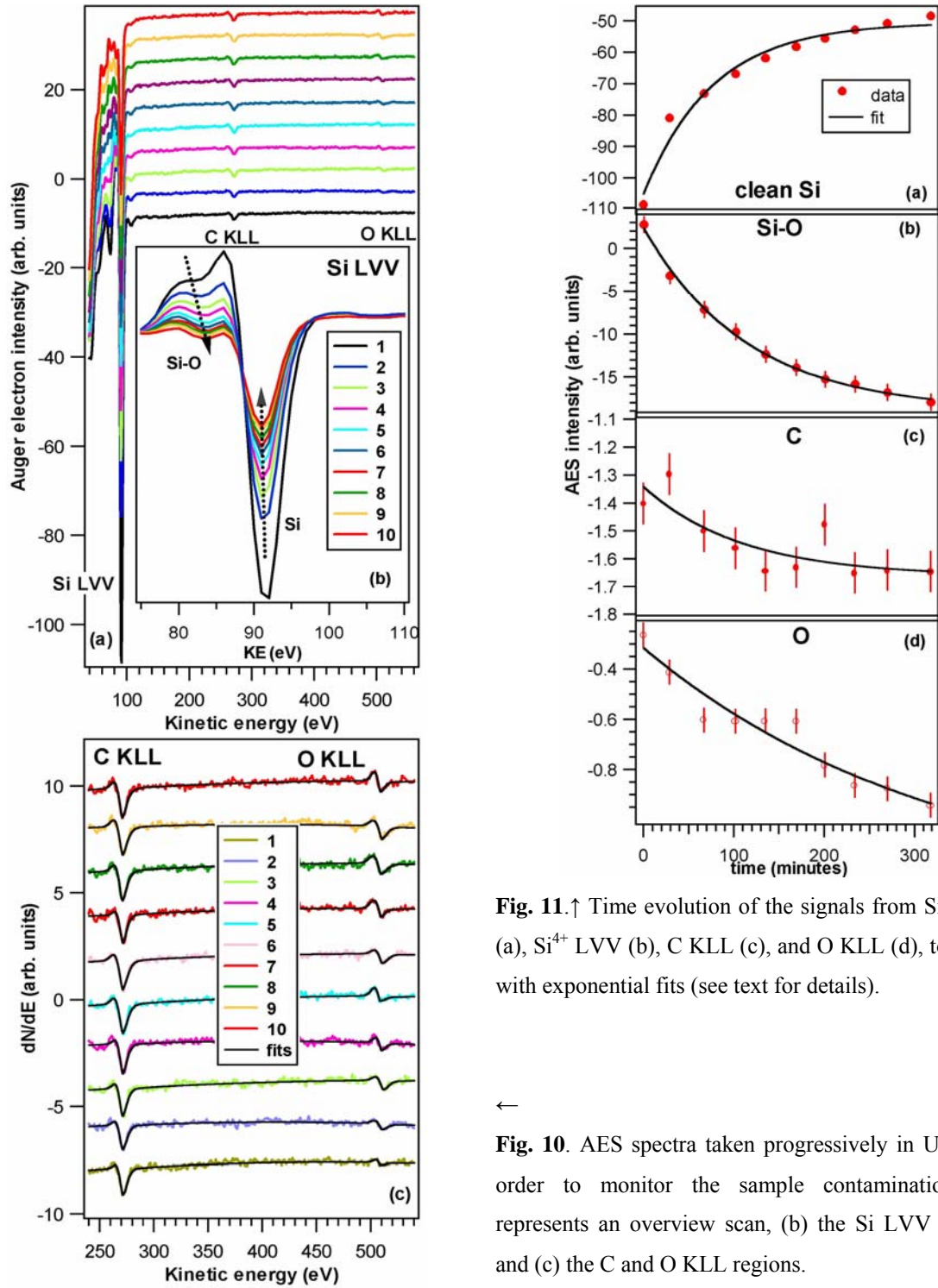


Fig. 11. ↑ Time evolution of the signals from Si⁰ LVV (a), Si⁴⁺ LVV (b), C KLL (c), and O KLL (d), together with exponential fits (see text for details).

←

Fig. 10. AES spectra taken progressively in UHV, in order to monitor the sample contamination. (a) represents an overview scan, (b) the Si LVV region, and (c) the C and O KLL regions.

Table 1. Values of parameters derived from the fitting of the temporal dependence of Auger signals

AES signal	$I(0)$ [arb.]	A [arb.]	τ [minutes]
Si^0 LVV	- 50.46	-54.58	76.16
Si^{4+} LVV	-18.90	+21.22	115.21
C KLL	-1.661	+0.320	109.89
O KLL	-1.319	+1.004	331.13

We suppose in the following that the remaining $I(0)$ peak, representing the Si^0 signal after waiting an infinite time with the sample in the UHV chamber, represents not clean silicon, but silicon bonded to carbon, or SiC. Formation of silicon carbide onto clean silicon was reported recently [40], but earlier studies evidenced contamination of Si(111) surfaces in ultrahigh vacuum and formation of SiC islands [9]. Also, the lineshape of the C KLL signal is quite similar to the lineshape of diamond-like nuclei on Si(001) and Si(111) [41]. In Fig. 12 we represent a detail of the Si^0 LVV signal from the spectrum of the clean sample and from the spectrum of the sample at the last AES scan.

A final remark is that even after 300 mins. of measurements plus 10-12 hours spent in the UHV chamber, the sample still exhibited a broad (1×1) LEED pattern and its cleaning was straightforward. This suggests that the silicon carbide-like compound formed at the surface exhibits long range order (results investigated also by STM and high resolution electron energy loss spectroscopy (HREELS) some years ago [9]).

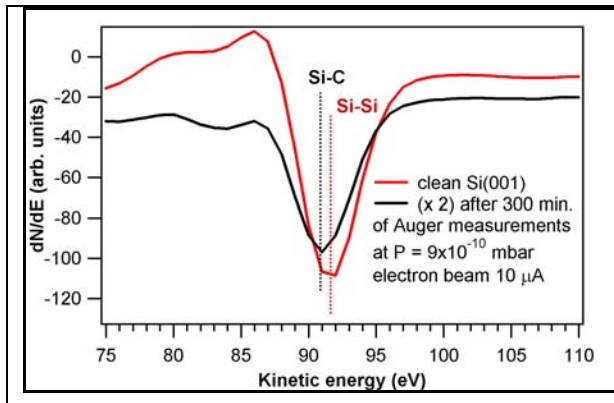


Fig. 12. Detail in the Si^0 AES signal with the spectrum of the clean sample and with the spectrum obtained after 300 mins of measurements in UHV under electron impact. The vertical lines represent estimated position of the AES minimum, attributed to clean silicon and to silicon reacted with carbon.

3.3. Growth of Fe on Si(001)

3.3.a. Structure and long range order. Fig. 13 presents the evolution of LEED patterns when the deposition is achieved at an elevated temperature (500 °C). The as-prepared sample

exhibits well-defined (2×1) and (1×2) reconstructions. As soon as Fe is deposited, the LEED pattern weakens and broadens and for 2.8 Å deposited, which represents roughly 2 single atomic layers of Fe, only a broad (1×1) pattern is visible. When the deposition is performed at room temperature, the LEED pattern disappears for the lowest quantity of Fe deposited, 0.7 Å, which roughly corresponds to half a monolayer.

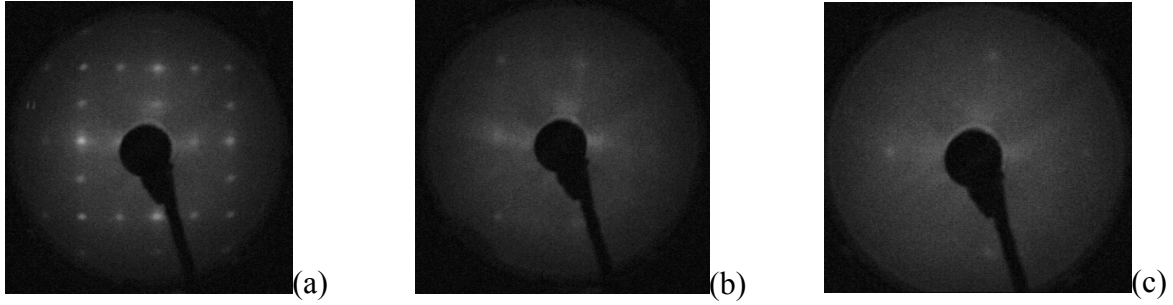


Fig. 13. Evolution of LEED patterns with Fe deposition at 500 °C. (a) clean Si(001); (b) 2.1 Å Fe deposited; (c) 8.4 Å Fe/Si(001).

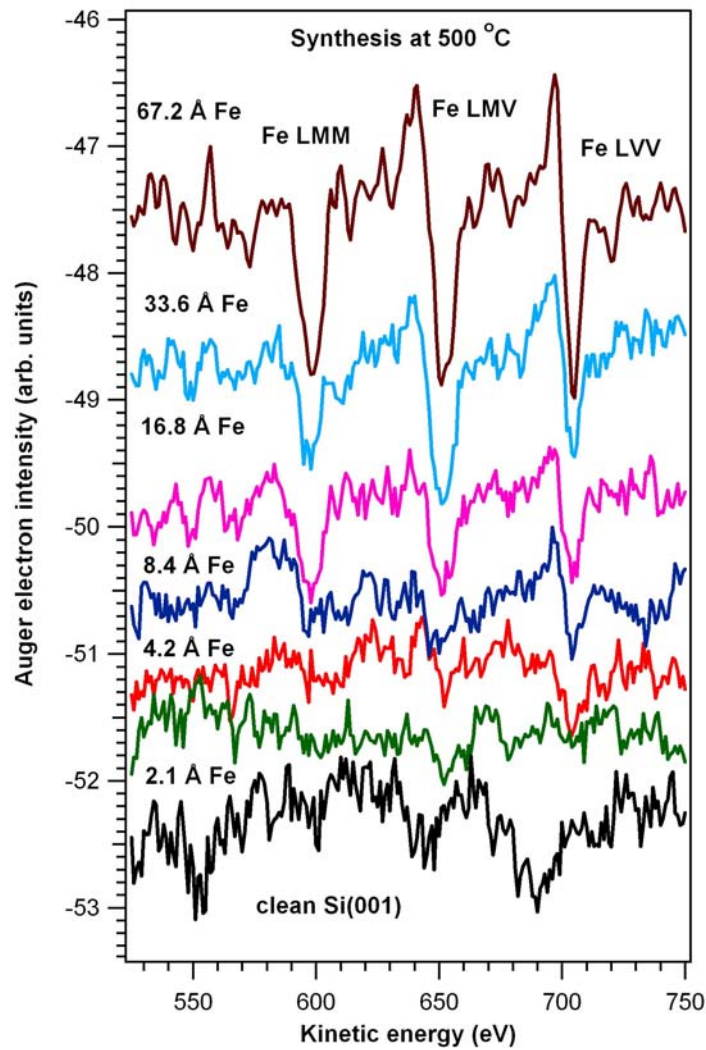


Fig. 14. Auger electron spectra of the Fe LMM, LMV, and LMV signals.

By considering the coherence length of about 25 nm corresponding to electrons of around 50 eV kinetic energy [42], this implies that at room temperature deposition islands with considerable lower lateral dimension are formed on the surface, with increasing surface roughness on the same order of magnitude.

3.3.b Intermixing and reactivity at the interface. Fig. 14 presents Auger electron spectroscopy (AES) results obtained from the Fe LMM-LMV-LVV lines for the samples synthesized at high temperature (500 °C). The electron inelastic mean free path (IMFP) is estimated at $9 \pm 2 \text{ \AA}$ in the latter case [43]. For the room temperature deposition, the IMFPs λ_{Si} and λ_{Fe} are close enough and also close to the accepted values for this energy range [43]. Consequently, one may infer that the Fe layer is situated over the Si substrate and that low intermixing occurs. There are some Si atoms diffused into the Fe layer.

3.3.c. Magnetic properties. Fig. 15 represents MOKE hysteresis loops obtained in both cases of room- and high-temperature. For samples synthesized at room temperature a detectable MOKE signal is observed. Moreover, this signal is different when the applied magnetic field is parallel to one of the $\langle 100 \rangle$ or to $\langle 110 \rangle$ directions. An uniaxial magnetic anisotropy is observed, although this sample did not exhibit any long range order. The Fe nanoparticles formed whose lateral dimensions are below 20 nm, are in well defined positions with respect to the the crystallographic axes of the substrate.

In the case of room temperature deposition, we obtained about 6 mdeg of MOKE signal, which corresponds to $2.4 \pm 0.6 \text{ nm}$ metal Fe layers. We may infer that the Fe layer is highly likely magnetic and the Fe average magnetic moment in this layer is close to the bulk value of $2.2 \mu_{\text{B}}$, or perhaps slightly less ($1.8\text{-}1.9 \mu_{\text{B}}$). This value is quite similar to the reported value of Fe layers on GaAs(001) or InAs(001), once the interface reaction ends [13].

For the sample synthesized at 500 °C, the saturation MOKE signal is one order of magnitude lower than at room temperature, whereas the estimated bulklike Fe layer is about 2 nm. Therefore, an average Fe atomic magnetic momentum of about $0.12 \pm 0.03 \mu_{\text{B}}$ is obtained in this case. This is about 5.4 % of the bulk Fe magnetic momentum. Therefore, we might infer that by depositing at high temperature some Fe is still magnetic, but with a very low magnetic momentum.

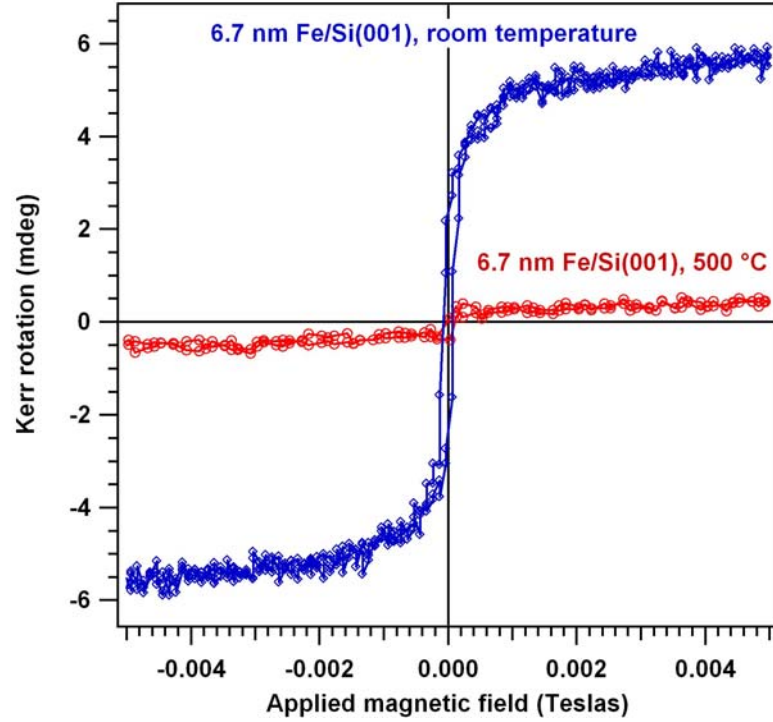


Fig. 15 MOKE hysteresis loops obtained on the samples synthesized (a) at room temperature and (b) at 500 °C.

4. Conclusions

The cleaning and contamination processes of Si(001) were reviewed by using a new MBE-XPS installation, permanently monitored by LEED, AES and RHEED. A huge kinetic energy shift of 15 eV was detected between the as-introduced sample and the sample when the cleaning procedure has started. A simple cleaning procedure consisting of successive annealings at not too elevated temperatures was set up, tested and proven. Fair LEED patterns were observed on the clean samples, with (2×1) - (1×2) reconstructions. Another result was the unexpected success in simulating Auger lineshapes with a convolution between a Beutler-Fano profile and a gaussian. The systematic study of sample contamination in ultrahigh vacuum exhibited the saturation-like behaviour of the oxidized silicon and of the oxygen signals; however, the evolution of the signal attributed to "clean" silicon cannot be explained unless one assumes that a quite similar energy is obtained from silicon reacted with carbon. In a partial pressure of some 3×10^{-10} mbar of contaminants, the sample is contaminated in slightly more than one hour. Therefore, the sample contamination is quicker than one expects, and the contamination rate, together with the measured partial pressures of contaminants, suggest a sticking coefficient close

to unity (assuming that 1×10^{-6} mbar corresponds roughly to a contamination of one atomic layer per second).

New results are also reported concerning the long range order, interface reactivity, and magnetic properties of Fe/Si(001). By growing at room temperature no long range order is detected; however, these small metal Fe particles exhibit noticeable ferromagnetism and uniaxial magnetic anisotropy. When the growth is performed at higher temperatures, Fe reacts completely with Si forming a long range ordered Fe silicide with weak, though detectable, ferromagnetism.

This study constitutes one of the rare ones combining MBE deposition with *in situ* AES and LEED characterization, and with *ex situ* magnetic. We do believe that the facts presented in the present paper will contribute to the elucidation of the interface formation in the highly studied Fe/Si(001) system.

Acknowledgements

This work was performed in the framework of the CNCSIS PCCE ID_76/2009 Project.

References:

- [1] A. Mascaraque, J. Avila, C. M. Teodorescu, M. C. Asensio, E. G. Michel, Phys. Rev. B **55**, R7315 (1997).
- [2] J. Avila, A. Mascaraque, C. Teodorescu, E. G. Michel, M. C. Asensio, Surf. Sci. **856**, 377 (1997).
- [3] J. Xu, W.J. Choyke, J.T. Tales Jr., J. Appl. Phys. **82**, 6289 (1997).
- [4] B. Sefsaf, B. Carrière, J.P. Deville, Microsc. Microanal. Microstruct. **3**, 15 (1992).
- [5] L. Viscido, J. M. Heras, J. Phys. Cd. Matter. **5**, A159 (1993).
- [6] J. Westermann, H. Nienhaus, W. Mönch, Surf. Sci. **311**, 101 (1994).
- [7] M. A. Zaïbi, J. P. Lacharme, C. A. Sébenne, Surf. Sci. **639**, 377 (1997).
- [8] M. G. Martin, J. Avila, M. Gruyters, C. Teodorescu, P. Dumas, Y.J. Chabal, M. C. Asensio, Appl. Surf. Sci. **156**, 123 (1998).
- [9] F. Xie, P. von Blanckenhagen, J. Wu, J.-W. Liu, Q.-Z. Zhang, Y.-C. Chen, E.-G. Wang, Appl. Surf. Sci. **139**, 181 (2001).
- [10] F. Shimoshikiryo, Y. Takakuwa, N. Miyamoto, Appl. Surf. Sci. **123**, 130 (1998).
- [11] R. Larciprete, E. Borsella, J. Electr. Spectrosc. Relat. Phenom. **76**, 607 (1995).
- [12] M. P. Cruz, J. A. Diaz and J. M. Siqueiros, Int. J. Mod. Phys. B **18**, 3169 (2004).

- [13] C. Teodorescu, F. Chevrier, V. Ilakovac, O. Heckmann, L. Lechevalier, R. Brochier, R.L. Johnson, K. Hricovini, Appl. Surf. Sci. **166**, 137 (2000); C.M. Teodorescu, F. Chevrier, R. Brochier, C. Richter, O. Heckmann, V. Ilakovac, P. De Padova, K. Hricovini, Surf. Sci. **482-485**, 1004 (2001); C.M. Teodorescu, F. Chevrier, R. Brochier, V. Ilakovac, O. Heckmann, L. Lechevalier, K. Hricovini, Eur. Phys. J. B **28**, 305 (2002); C.M. Teodorescu, D. Luca, Surf. Sci. **600**, 4200 (2006).
- [14] J.M. Gallego, J.M. García, J. Alvarez, R. Miranda, Phys. Rev. B **46**, 13339 (1992).
- [15] F. Zavaliche, W. Wulfhekel, H. Xu, J. Kirschner, J. Appl. Phys. **88**, 5289 (2000).
- [16] I.I. Pronin, M.V. Gomoyunova, D.E. Malygin, D.V. Vyalikh, Y.S. Dedkov, S.L. Molodsov, J. Appl. Phys. **104**, 104914 (2008).
- [17] I.I. Pronin, M.V. Gomoyunova, D.E. Malygin, D.V. Vyalikh, Y.S. Dedkov, S.L. Molodtsov, Appl. Phys. A **94**, 467 (2009).
- [18] M. Verziu, J. El Haskouri, D. Beltran, P. Amoros, D. Macovei, N.G. Gheorghe, C.M. Teodorescu, S.M. Coman, V. I. Parvulescu, Top. Catal. **53**, 763 (2010).
- [19] A.N. Parvulescu, D. Mores, E. Stavitski, C.M. Teodorescu, P.C.A. Bruijninx, R.J.M. Klein Gebbink, B.M. Weckhuysen, J. Amer. Chem. Soc. **132**, 10429 (2010).
- [20] A. Negoï, S. Wuttke, E. Kemnitz, D. Macovei, C. M. Teodorescu, V.I. Parvulescu, S.M. Coman, Angew. Chem. Intl. Ed. **49**, 8134 (2010).
- [21] F. Neatu, L. Protesescu, M. Florea, V.I. Parvulescu, C.M. Teodorescu, N. Apostol, P.Y. Toullec, V. Michelet, Green Chemistry **12**, 2145 (2010).
- [22] C.M. Teodorescu, G. Socol, C. Negri, D. Luca, D. Macovei, J. Exper. Nanosci. **5**, 509 (2010).
- [23] I. Enculescu, E. Matei, V. Vasilache, C.M. Teodorescu, phys. stat. sol. (a) **207**, 2517 (2010).
- [24] J. Neamtu, G. Georgescu, T. Malaeru, N.G. Gheorghe, R.M. Costescu, I. Jitaru, J. Ferré, D. Macovei, C.M. Teodorescu, Digest J. Nanomater. Biostr. **5**, 873 (2010).
- [25] D. Mardare, V. Nica, V. Pohoata, Dan Macovei, N. Gheorghe, D. Luca, C.M. Teodorescu, Thin Solid Films, *accepted* (2010).
- [26] N.G. Gheorghe, R.M. Costescu, C. M. Teodorescu, Physica E: Low-dimensional Systems and Nanostructures, *submitted* (2010).
- [27] I. Stavarache, A.M. Lepadatu, N.G. Gheorghe, R.M. Costescu, G. Stan, D. Marcov, A. Slav, G. Iordache, T.F. Stoica, V. Iancu, V.S. Teodorescu, C.M. Teodorescu, M.L. Ciurea, J. Nanopart. Res. **13**, 231 (2011).
- [28] G.A. Lungu, D. Macovei, C.M. Teodorescu, Digest J. Nanomater. Biostr. **5**, 85 (2010).

- [29] M. Cernea, B.S. Vasile, P. Ganea, R. Radu, V. Mihalache, A. Husanu, J. Amer. Ceramic Soc. **94**, 736 (2011).
- [30] A.C. Galca, V. Stancu, M.A. Husanu, C. Dragoi, N.G. Gheorghe, L. Trupina, M. Enculescu, E. Vasile, Appl. Surf Sci., accepted (2010), doi:10.1016/j.apsusc.2011.01.056.
- [31] I. Pintlilie, C. M. Teodorescu, F. Moscatelli, R. Nipoti, A. Poggi, S. Solmi, L. S. Løvlie and B. G. Svensson, J. Appl. Phys. **108**, 024503 (2010).
- [32] P. Palade, G.A. Lungu, A.M. Husanu, J. Alloys Compds. **505**, 343 (2010).
- [33] C. Teodorescu, F. Chevrier, V. Ilakovac, O. Heckmann, L. Lechevalier, R. Brochier, R.L. Johnson, and K. Hricovini, Appl. Surf. Sci. **166**, 137 (2000).
- [34] D. Briggs, M. P. Seah, eds., *Practical Surface Analysis by Auger and X-ray Photoelectron Spectroscopy*, Wiley, New York (1983).
- [35] Y. Enta, S. Suzuki, S. Kono, T. Sakamoto, Phys. Rev. B **39**, 5524 (1989).
- [36] C. M. Teodorescu, J. M. Esteva, R. C. Karnatak, A. El Afif, Nucl. Instrum. Meth. Phys. Res. A **345**, 141 (1994).
- [37] C. M. Teodorescu, J. M. Esteva, R. C. Karnatak, A. El Afif, M. Womes, J. Phys. B: At. Mol. Opt. Phys. **30**, 4293 (1997).
- [38] J. P. Connerade, A. M. Lane, Rep. Prog. Phys. **51**, 1439 (1988)
- [39] C. Coletti, C. L. Frewin, S. E. Sadow, M. Hetzel, C. Virojanadara, U. Starke. Appl. Phys. Lett. **91**, 061914 (2007).
- [40] J. K. Simons, R. V. Duevel, S. P. Frigo, J. W. Taylor, R. A. Rosenberg, J. Appl. Phys. **76**, 5481 (1994).
- [41] M.G. Martin, J. Avila, M. Gruyters, C. Teodorescu, P. Dumas, Y.J. Chabal, M.C. Asensio, Appl. Surf. Sci. **123**, 156 (1998).
- [42] S. Hüfner, *Photoelectron spectroscopy. Principles and applications*, 3rd Ed. (Springer, Berlin, 2003).